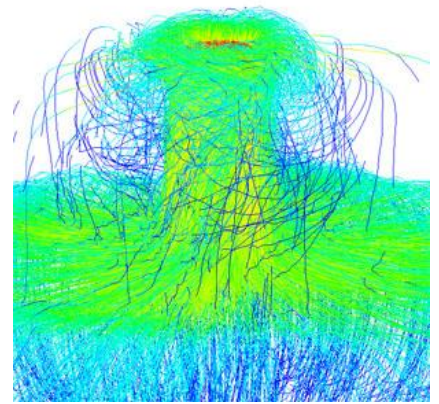


Automotive Rotary-Bell Spray Painting

Modelling and Simulation



Lucas Ariel Martinez

Degree project for Master of Science (Two Years) in

Complex Adaptive Systems

30 hec

Department of Physics

University of Gothenburg



UNIVERSITY OF GOTHENBURG

Faculty of Science

Abstract

The Electrostatic Rotary Bell Sprayer (ERBS) technique is a painting process where a high-speed rotating device with high electric potential atomizes the paint producing charged droplets and sprays them through the air onto a surface. These devices commonly use a shaping-air system, which in conjunction with the electrostatic forces present, direct the particles to the target.

In industries with high volume production environments, like the automotive industry, there is a tendency towards the use of this highly automated painting technique because of its superior transfer efficiency and high-quality finishing.

In the present research, IBOFlow, a Computational Fluid Dynamics (CFD) solver developed at the Fraunhofer-Chalmers Centre (FCC) is employed to perform simulations on an ERBS system. The results are then compared with empirical measures obtained at the Swerea IVF research laboratories looking for validation. Subsequently, the focus is set specifically on simulating the region near the applicator bell. By accurately simulating this region a good understanding of the active processes close to the bell can be gained. For this purpose, a framework was created to analyse and collect fluid and particle statistics, sampled over a plane close to the bottom of the bell. This information is then stored and readily available to use as input conditions for coarser simulations over larger areas, which can include the target to be painted, without the extra difficulties and costs of having to take into consideration the complicated physics present in the near-bell region.

Acknowledgements

This research project would not have been possible without the help and support of many people.

First of all I want to express my gratitude to Associate Professor Fredrik Edelvik and project manager Dr. Johan Carlson for giving me the opportunity to work on the interesting topic of automotive rotary-bell spray painting, and for the advice and review of various materials.

I owe my deepest gratitude to Lic. Björn Andersson, my supervisor at the FCC, for his constant guidance and assistance during my project. This thesis would have remained a dream had it not been for all his help, stimulating ideas and clarifications. I also thank him for all the patience that he had me, answering all my questions (and even the same questions twice), be them about Linux, physics or administrative paperwork.

I am also most grateful to Dr. Andreas Mark, who was also following my work very closely, for his instructive and helpful explanations, and for his invaluable assistance especially when it concerned IBOFlow. He has been always willing to lend me a hand despite his already very full agenda.

I am very much thankful to Professor Lars Davidson, my examiner at the Department of Fluid Dynamics at Chalmers, for all his support and encouragement.

I wanted also to extend my thanks to Professor Bernhard Mehlig, for introducing me to Björn, and consequently to this project.

I consider it an honour to have been part of the very knowledgeable team at the FCC, and having worked alongside some very talented people. I wish to thank all of them for creating a warm and relaxed atmosphere, making it a great place to work. I cannot acknowledge all of them properly, but I hope that everyone who has influenced me feels the satisfaction of having helped me complete this thesis. However, I would like to make a special mention of Anders Ålund for all his patience regarding my continuous demand of more storage space.

I am truly indebted to the European Commission, for implementing such a wonderful programme like the Erasmus Mundus scholarships, without which I could have never afforded the incredible opportunity to study in Europe.

I will forever be thankful to my wonderful family for giving me unconditional love and care; and for always believing in me and being a constant source of encouragement. Even though they are far away, they are always present in my heart, and I know I can always count on them when times are rough.

Last, but by no means least, I wanted to thank my beloved girlfriend for unconditionally loving me through good and bad times, and always having faith in me. She has been a great supporter during this period, inspiring confidence in me and cheering me up when I was depressed, especially during this difficult year that we have been apart. There are no words to express how much I love her and how happy she makes me feel.

This work has been conducted within the Virtual Paint Shop project with the partners Volvo Cars, SAAB Automobile, Scania, Volvo AB, Swerea IVF, Konga Bruk and General Motors NA. It was supported in part by the Swedish Governmental Agency for Innovation Systems, VINNOVA. The support is gratefully acknowledged.

Table of Contents

1	Introduction	1
1.1	Introduction	1
1.2	Motivation.....	2
2	Background	3
2.1	Rotary bell applicator assemblies	3
2.2	Physical phenomena involved in ERBS.....	5
2.2.1	The near-bell region.....	5
3	The model	8
3.1	Governing Equations.....	8
3.1.1	Fluid Equations.....	8
3.1.2	Electrostatic Equations	9
3.1.3	Particle Equations	9
3.2	FCC's IBOFlow	11
3.3	Present approach.....	13
4	Experimental setup	15
5	Computer simulations setup.....	19
5.1	Part I: Near-Bell Simulations	19
5.2	Part II: Framework to analyse the Near-Bell Simulations	23
5.3	Part III: Far-Field Simulations	24
6	Results and Discussion	26
6.1	Near-bell simulation.....	26
6.2	Python framework analysis.....	29
6.3	Far-field simulation	33
7	Conclusion.....	34
8	Future work.....	35
	Bibliography	36

1 Introduction

1.1 Introduction

The painting process in the industry is currently highly automated, and in particular, in the automotive industry, the painting of cars is commonly performed using the spray painting technique. The paint applicators most widely used for high-quality finishing are the Electrostatic Rotary Bell Sprayers, because they provide a very uniform paint film thickness and good transfer efficiency. This is attained due to a shaping air system which directs the paint droplets towards the target, helped by an additional electrostatic field which further supports the droplet transport.

A better understanding of the electrostatic spray painting dynamics is required in order to improve the transfer efficiency and the finish quality of electrostatic high-speed rotary bell atomizers. In order to validate the physical models of an ERBS applicator, a detailed characterization of the processes involved is needed, among which we can mention: the atomization of the paint at the bell cup and the initial break-up of the particles, the two-way interaction between the particles, the shaping airflow and the electric field, and the droplets deposition and paint layer formation at the workpiece's surface.

This work presents a small background of the spray painting technique and briefly describes the current challenges faced to develop and validate one single model which includes all the physical aspects present in the electrostatic spray painting method. Next, a model of the whole painting process is constructed using a powerful CFD solver (IBOFlow) developed at the FCC, tuning the parameters of the simulations to try to replicate the atomization conditions that best approximate the measurements.

Subsequently the model is validated by running simulations and comparing the results with the real measures. Once these results approximate the measures from the experiments, the focus of the current work is redirected to just a small area of the painting process, namely, the near-bell region. The objective is to obtain important information in this area, so that it can be analysed and processed to be later used as input parameters to construct coarser simulations. In this way, larger simulations can be run without having to recur to the costly and complicated measurement techniques of the initial conditions.

In summary, it can be said that the aim of this study is twofold. First, to gain a better understanding of the paint transfer process, with the purpose of reducing the current rudimentary "trial-and-error" approaches in the industry. And second, to provide data for further model development by collecting near-bell statistics with the intention to reduce the dependence on empirical databases.

1.2 Motivation

The paint transfer efficiency, or deposition ratio, is defined as the ratio between the amount of paint deposited on the target, and that which has been sprayed from the applicator. Understandably, this metric is of primary concern to measure the efficiency of the painting process.

Due to the superiority of ERBS applicators over ordinary paint guns in terms of transfer efficiency, spray pattern consistency, and low compressed air consumption, the use of these types of applicators has been growing among the industries with high volume production environments. However, these systems are not perfect and they also have some drawbacks. They produce a certain amount of overspray, and there is also some rebound from the sprayed surface. Therefore, they are unable to transfer a substantial portion of the paint to the target.

One of the leading industries which pioneered this tendency towards ERBS applicators and is actively seeking to improve their performance is the automotive industry. The real transfer efficiency depends not only on the technique employed and the characteristics of the atomizer, but also on a big number of other factors, including the desired quality of finishing, film thickness, uniformity of the paint (i.e. accumulation of paint on the edges due to electrostatic effects attracting particles that would normally pass by the side of the workpiece), etc. On average, the current transfer efficiency attained by ERBS systems in the automotive industry is around 75%, while if they were to operate in ideal conditions they could achieve transfer efficiencies of over 90%. This means that there is still a great need for improvement in this area.

The paint process is a very expensive part of an automotive company's manufacturing facility, and even a small improvement in the transfer efficiency of only 1% can result in significant costs and time savings. Increasing the transfer efficiency would not only reduce the amount of paint needed in the process, but would also reduce the paint sludge production along with the associated after treatment and disposal costs. Moreover, it would imply a reduction of the air turbine usage, and thus profiting from the savings due to the lower energy consumption. Additionally, this improvement in the energy efficiency, plus the reduction in the amount of volatile organic compounds emitted due to less overspray, could be regarded as a step forward into an environmentally friendly policy, further contributing to enhance the company's image.

The current challenge faced by the automotive industry is therefore to increase the paint transfer efficiency and to reduce the volatile emissions, preserving the finish quality and line speed. In this regard is where simulations play a crucial role. In ERBS painting systems several parameters have important influences in the transfer efficiency. Consequently, being able to predict with good accuracy the individual effects of these parameters in the transfer process is of utmost importance. Computer simulations would enable us to gain a better understanding of the effects of each parameter, which in turn will allow us to improve the design of these kinds of systems, increasing their performance to achieve higher efficiencies. Additionally, they would help to reduce the amount of physical experiments required for new set-ups, significantly decreasing the time needed to introduce new car models into the market.

2 Background

2.1 Rotary-Bell Applicator Assemblies

A typical rotary bell applicator consists of the following major assemblies:

- The valve module, which consists of the passages for paint, solvent, and compressed air, and the valves to control their flow into the system, for paint delivery, cleaning and purging with solvent, and management of compressed air to the valves, turbine, and shaping air shroud.
- The bell cup, which is a conical disc fixed to the shaft of the turbine (the robot arm). The paint is injected into the centre of the rear of the disc, forming a film at the bottom. The centrifugal forces then pull the paint towards the edges of the cup, where it breaks into atomized droplets.
- The turbine, which is a high speed air motor that rotates the bell cup at speeds ranging from 10,000rpm to 70,000rpm, depending on the cup diameter, atomization desired, and physical properties of the paint.
- The shaping air shroud, or shaping air ring, is a ring with small passages (pinholes) for air to flow out of the front of the atomizer, outside of the bell cup diameter, to control the size of the spray pattern produced. In general, as more air is pushed through the shroud, the atomized paint will be shaped into a smaller pattern.
- The electrostatic system, which can be internal or external, depending on whether the charge is applied directly or indirectly to the paint particles. In the internal or direct method, a high voltage charge (usually between 20,000 to 90,000 volts DC) is supplied to the applicator, which has the effect of charging the paint before it is atomized. On the other hand, in the external or indirect method, the high voltage is supplied to a series of 4-8 forward facing electrodes placed in a circular array around the bell cup. This has the effect of ionizing the air in their surroundings, charging the paint droplets as they flow through this region (due to the free ions). The internal charging method works well with solvent-based paints due to the low conductivity of the solvent. On the contrary, water-based paints require the use of an external charging, or otherwise, the isolation of the entire circulation system. In both cases, the paint particles are negatively charged while the target is charged with positive energy or grounded, resulting in electrostatic attraction between the atomized paint and the workpiece. Furthermore, the electrically charged particles repel each other and spread themselves more evenly as they exit the spray nozzle. Figure 2.1 and Figure 2.2 illustrate the process of internal charging and external charging of paint droplets, respectively.

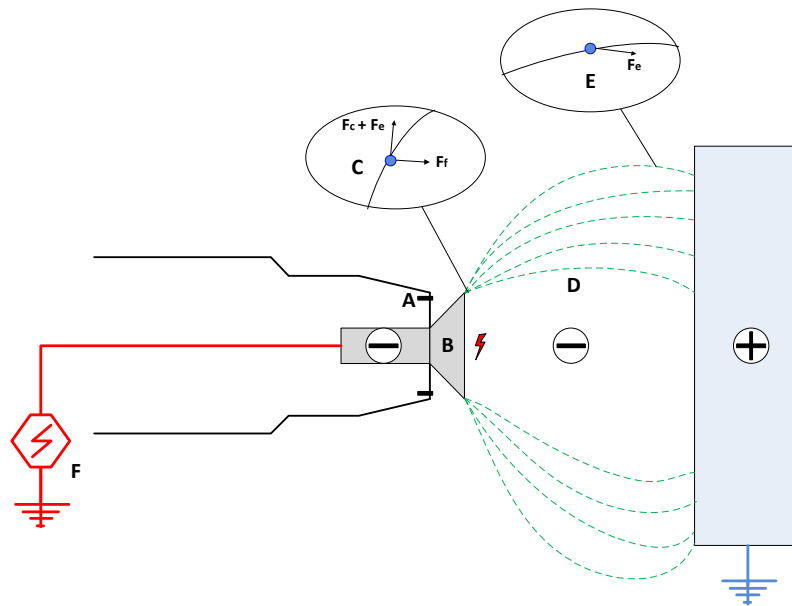


Figure 2.1: A sketch of the internal charge process. The electrostatic charge is made thanks to the built-in cascade. The paint acquires its electric charge from the edge of the bell cup. (A) Shaping air shroud. (B) Negatively charged bell charges the particles. (C) Centrifugal and electrostatic forces (repulsion from the bell); and the air flow force (directing towards the target). (D) Electric field. (E) Electrostatic force (attraction close to the target). F: High voltage generator.

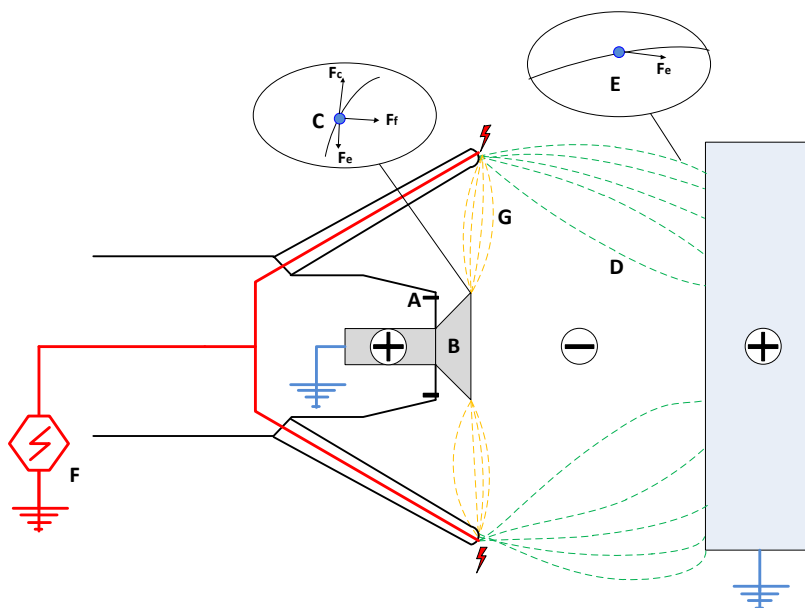


Figure 2.2: A sketch of the external charge process. The paint particles are charged with ions passing close to the external electrodes through the electric field. When an ion encounters a particle, it binds to its surface and cannot be detached from it. (A) Shaping air shroud. (B) Grounded (positively charged) bell. (C) Centrifugal and electrostatic forces (attraction from the bell as the particles absorb negative charges from the air); and the air flow force (directing towards the target). (D) Electric field. (E) Electrostatic force (attraction close to the target). (F) High voltage generator. (G) Ions in the air charge the particles.

2.2 Physical Phenomena Involved in ERBS

This section provides an overview of the physical phenomena present in an ERBS painting process, and describes the typical characteristics exhibited by different regions of the system.

Three different regions can roughly be identified in the ERBS painting process: the region near the bell, the region close to the target, and the region in between those two. The near-bell region is characterized by physical phenomena like the atomization of the paint into droplets, and the forces of the electrostatically charged particles, repelling each other. The region near the target is characterized by the transfer efficiency, and the influence that both the downdraft and the electrostatic attraction have on the deposition of the paint droplets into the workpiece surface and over-spray. The region between the bell applicator and the target is called the transport field and it is the largest of the regions. It includes the physics for the shaping-air flow, the turbulent flow developed, the electrostatic field, and the dynamics of the particles.

The spray dynamics combined with the electric field and with the swirling turbulent flow induced by the ERBS applicator is a very complicated phenomenon. The electric field interacts with the charged paint particles, while these in turn interact with the shaping airflow via mass, momentum and energy exchange. That is, the motion of the particles is influenced by the drag force of the airflow, the electrostatic force of the electric field, and the repulsive forces of other charged particles. At the same time, the electric field is influenced by the motion of the charged particles, and the flow field is influenced by the drag force of the moving particles. We can see then, that an indirect interaction between the electric field and the flow field is created, which further complicates the matter. The interactions between the three main components of the transport field can be seen in Figure 2.3.

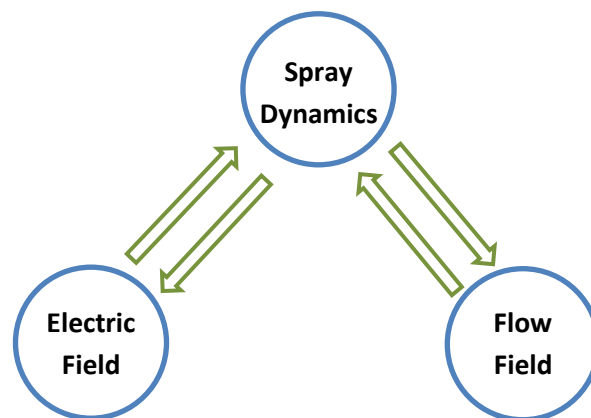


Figure 2.3: Interactions of the three main processes in the transport field.

2.2.1 The Near-Bell Region

The region close to the applicator has a particular importance since it is the least understood of all three. It is strongly turbulent and completely filled with paint particles. The interactions between particles, due to the electrical repellent forces, are especially important in this area, however, the

huge amount of them present in this zone, make the calculations very computationally expensive and time-consuming to resolve.

Yet an even more difficult challenge is posed by the modelling and simulation of the paint atomization. This is the reason why current studies always use empirical measures for the initial droplet distribution, despite how difficult and costly it is to perform these measurements, and that special equipment is required to perform them.

The atomization process of paint into droplets can be subdivided into two stages, that is, the primary atomization and the secondary atomization, or break-ups. In the primary atomization step, due to the centrifugal force, the paint is propelled out of the bell through the serrations present at the edge. These small channels at the bell rim force the paint into large and thin liquid structures which resemble filaments. When the filaments come into contact with the air they have a large relative velocity compared to it. This creates instability waves in the surface of the paint, causing them to break-off and giving place to the second stage of the process, the secondary break-up.



Figure 2.4: The bell's edge is the black zone to the left, and from it emanates the threads of paint, or "filaments". These filaments begin to break a few millimetres away from the edge. Photograph courtesy of Swerea IVF.

The secondary atomization step is the subsequent break-up of the paint threads into smaller structures and it finishes when the paint droplets reach a stable size. Whether a drop of liquid divides further into multiple droplets or eventually compresses lengthwise to form a single drop depends on the density, viscosity, and surface tension of the liquid, and on the initial dimensions of the filament.

Since distinct physical processes are involved in each regime, different modelling strategies are needed. In particular, the dynamics of the phase interface taking place during the primary break-up are highly complex, not well understood, and remain an unresolved problem in the area of atomization simulation [1].

In the present study, computer simulations of ERBS painting processes do not include a primary atomization model, since the current version of the IBOFlow software developed at the FCC does not include one yet [2] [3]. Instead, initial distributions for the droplet sizes and velocities very close to the bell are still required. However, the initial droplets do undergo the secondary atomization process, which is effectively implemented in IBOFlow and simulated using the Taylor Analogy Breakup model [4].

3 The Model

3.1 Governing Equations

3.1.1 Fluid Equations

The motion of fluid substances is described by the Navier-Stokes equations. These equations arise from applying Newton's second law to fluid motion, together with the assumption that the fluid stress is the sum of a diffusing viscous term, which is proportional to the gradient of velocity, plus a pressure term. A solution of the Navier-Stokes equations is called a velocity field or flow field, which is a description of the velocity of the fluid at a given point in space and time. Once the velocity field is solved for, other quantities of interest may be found, such as the flow rate or the drag force.

The Navier-Stokes equations might be simplified when considering an incompressible flow of a Newtonian fluid. Taking the incompressible flow assumption into account and assuming constant viscosity, the Navier–Stokes equations read, in vector form:

$$\rho_f \frac{\partial \vec{u}}{\partial t} + \rho_f \vec{u} \cdot \nabla \vec{u} = -\nabla p + \mu \nabla^2 \vec{u} + \vec{s} \quad (3.1)$$

Where \vec{u} is the fluid velocity, ρ_f is the fluid density, p is the pressure, μ is the dynamic viscosity of the fluid, and \vec{s} represents other forces acting on the fluid, per unit volume, like for example, gravity. In this case \vec{s} can also be referred to as the droplet source term, since the paint droplets are the mayor contributors to this force, affecting the air because of their motion and electric charge.

If temperature effects are also neglected, only one more equation is needed to close the system, apart from the boundary conditions. That is the mass continuity equation, which is a statement of the conservation of volume. Under the incompressibility assumption, density is a constant and it follows that the equation simplifies to:

$$\nabla \cdot \vec{u} = 0 \quad (3.2)$$

In Cartesian coordinates, the equations read:

$$\frac{\partial u_j}{\partial x_j} = 0 \quad (3.3)$$

$$\rho_f \frac{\partial}{\partial t} u_i + \rho_f u_j \frac{\partial u_i}{\partial x_j} = -\frac{\partial p}{\partial x_i} + \frac{\partial}{\partial x_j} \left(\mu \frac{\partial u_i}{\partial x_j} \right) + \rho_f g_i \quad (3.4)$$

where g_i is the gravitational acceleration.

3.1.2 Electrostatic Equations

The electric field, generated due to the potential difference between the applicator, negatively charged, and the workpiece, grounded, can be described by Poisson's equation, which provides a relationship between the potential ϕ and the space charge density ρ :

$$\nabla^2 \phi = -\frac{\rho}{\varepsilon} \quad (3.5)$$

where ε is the air electrical permittivity.

The electric field is given by the gradient of the potential:

$$\vec{E} = -\nabla\phi \quad (3.6)$$

3.1.3 Particle Equations

The motion of particles is described by solving a set of ordinary differential equations, calculating the particle velocity and position at every instant. The equation of motion includes the forces of: buoyancy/gravity, fluid (due to the pressure gradient and viscous stresses), added-mass, Stokes drag, electromagnetic and Basset forces. In the present work, the effect of the Basset force is not considered, since it is always an order of magnitude smaller than the buoyancy and Stokes drag. The fluid forces due to, for example, difference in pressure, are also not considered, given that the particles are considered as points and thus there cannot be a pressure drop at different sides of the particle. With these simplifications, the motion equation based on the Maxey and Riley [5] formulation is:

$$\vec{F}_d(\vec{u}_r) = m_p \frac{\partial^2 \vec{x}}{\partial t^2} = m_p \frac{\partial \vec{u}_p}{\partial t} \quad (3.7)$$

where \vec{x} is the particle's position vector, $m_p = \rho_p V_p$ is the mass of the particle, equal to the product of its density and volume, and $\vec{u}_r = \vec{u}_f - \vec{u}_p$ is the relative velocity vector between the particle and the fluid.

The force \vec{F}_d acting on the particles is then the sum of the following forces:

$$\text{Stokes drag} = \frac{3}{4} C_d \frac{\rho_f}{\rho_p} \frac{m_p}{2a} |\vec{u}_r| \vec{u}_r \quad (3.8)$$

$$\text{Buoyancy} = (\rho_p - \rho_f) V_p \vec{g} \quad (3.9)$$

$$\text{Added mass} = \frac{\rho_f V_p}{2} \frac{\partial \vec{\mathbf{u}}_r}{\partial t} \quad (3.10)$$

$$\text{Electromagnetic forces} = \vec{\mathbf{E}} q_p \quad (3.11)$$

Resulting in:

$$\vec{\mathbf{F}}_d = \frac{3}{4} C_d \frac{\rho_f}{\rho_p} \frac{m_p}{2a} |\vec{\mathbf{u}}_r| \vec{\mathbf{u}}_r + (\rho_p - \rho_f) V_p \vec{\mathbf{g}} + \frac{\rho_f V_p}{2} \frac{\partial \vec{\mathbf{u}}_r}{\partial t} + \vec{\mathbf{E}} q_p \quad (3.12)$$

where ρ_p is the particle (paint) density, ρ_f is the fluid (air) density, a is the radius of the particle, V_p is the volume of the particle, m_p is the mass of the particle, q_p is the particle charge, $\vec{\mathbf{E}}$ is the electric field, and C_d is the drag coefficient, which depends on the Reynolds number of the particle Re_p and has the following empirical correlation [6] [7] [8]:

$$C_d = \begin{cases} 24 \frac{1 + 0.15 Re_p^{0.687}}{Re_p} & \text{for } Re_p \leq 1000 \\ 0.44 & \text{for } Re_p > 1000 \end{cases} \quad (3.13)$$

$$\text{where } Re_p = \frac{2a |\vec{\mathbf{u}}_r| \rho_f}{\mu_f}$$

where μ_f is the dynamic viscosity of the fluid (air).

This formula for the drag coefficient closely approximates the measured empirical values except for high Reynolds numbers. The departure from the empirical curve occurs roughly around $Re = 1200$. For that reason, in equation (3.13), the minimum value for the drag coefficient is fixed to be 0.44 for Reynolds numbers higher than 1000.

Inserting equation (3.7) into equation (3.12), and replacing $\vec{\mathbf{u}}_r$ by $\vec{\mathbf{u}}_f - \vec{\mathbf{u}}_p$ the following differential equation is obtained:

$$\frac{\partial \vec{\mathbf{u}}_p}{\partial t} = \frac{3}{4} \frac{C_d}{2a} \frac{\rho_f}{\rho_p} |\vec{\mathbf{u}}_f - \vec{\mathbf{u}}_p| (\vec{\mathbf{u}}_f - \vec{\mathbf{u}}_p) + \frac{(\rho_p - \rho_f)}{\rho_p} \vec{\mathbf{g}} + \frac{\rho_f}{2\rho_p} \frac{\partial (\vec{\mathbf{u}}_f - \vec{\mathbf{u}}_p)}{\partial t} + \frac{\vec{\mathbf{E}} q_p}{m_p} \quad (3.14)$$

Finally, isolating the differential term of the particle's velocity on one side of the equation, the final expression for the motion equation implemented is attained:

$$\frac{\partial \vec{\mathbf{u}}_p}{\partial t} \left(1 + \frac{\rho_f}{2\rho_p} \right) = \frac{3}{4} \frac{C_d}{2a} \frac{\rho_f}{\rho_p} |\vec{\mathbf{u}}_f - \vec{\mathbf{u}}_p| (\vec{\mathbf{u}}_f - \vec{\mathbf{u}}_p) + \left(1 - \frac{\rho_f}{\rho_p} \right) \vec{\mathbf{g}} + \frac{\rho_f}{2\rho_p} \frac{\partial \vec{\mathbf{u}}_f}{\partial t} + \frac{\vec{\mathbf{E}} q_p}{m_p} \quad (3.15)$$

It is easy to see from the left side of this equation how the particle is accelerated as if it had an added mass of half of the fluid it displaces, and on the right side, there is the additional force contribution due to the acceleration of the fluid. To see this even clearer, we can rewrite equation (3.15) as:

$$\left(1 + \frac{\rho_f}{2\rho_p}\right) \frac{\partial \vec{u}_p}{\partial t} = \sum \frac{\mathbf{F}_o}{m_p} + \left(\frac{\rho_f}{2\rho_p}\right) \frac{\partial \vec{u}_f}{\partial t} \quad (3.16)$$

where \mathbf{F}_o is the sum of the other forces previously mentioned. In this case, however, the added mass force is rather small, since the density of the paint is much bigger than the density of the air and thus $\rho_f/\rho_p \ll 1$.

To compute equation (3.15), the values for the fluid velocity field and the electric field are required at the exact positions of the particles. These values then need to be interpolated from their calculated values at the grid points. In turn, the resulting drag force and charge at the positions of the particles are interpolated back to the grid points, constituting the droplet source term of the Navier Stokes' equation (3.1), and the spatial charge density of the Poisson's equation (3.5). The particle charge is assumed to be proportional to the square of its radius, and this area charge density has been determined empirically by plate simulations [9].

3.2 FCC's IBOFlow

IBOFlow [10] [3] [4] is the name of the CFD solver developed entirely in-house at the FCC. The name stands for "Immersed Boundary Octree Flow Solver" and it was designed to solve complex flows such as multiphase and free surface flows, and moving and interacting bodies. Moreover, in the specific case of ERBS painting simulations, it can also solve the electric field.

IBOFlow is an incompressible fluid solver based in the finite-volume discretization method, guaranteeing both global and local conservation of mass. The incompressible Navier-Stokes' equations, which express the conservation of momentum and mass, are coupled with the SIMPLEC method for the pressure correction. The SIMPLEC algorithm is an improved variant over the original SIMPLE algorithm. In the latter, the influence of the neighbouring velocities is neglected in the velocity correction equations, while in the former they are approximated. To close the Navier-Stokes equations governing the motion of the fluid, IBOFlow offers different choices of boundary conditions which are employed at the boundaries of the fluid domain.

The solver also implements a unique immersed boundary (IB) method, the Mirroring IB Method [11] [12]. This method is three-dimensional, has second-order accuracy in space, and is implicitly formulated. It uses an IB condition to mirror the velocity field along the normal of the triangulated IB surface, so that the fluid follows it precisely. A special treatment is adopted to account for this fictitious velocity field inside the IB, so that no mass flux is present over the boundary.

Additionally, IBOFlow uses a Cartesian octree grid to discretize the computational domain, which can be dynamically refined by recursively subdividing cells into eight octants. In a similar way it also allows for dynamic coarsening when less level of detail is required. The specified refinement level of the grid for a certain zone indicates the total number of refinements that the zone should have with respect to the base cell size, whether that implies performing more refinements on the cells or merging cells together for a coarser grid. This flexibility in the meshing facilitates the treatment of moving and interacting objects in the fluid, while saving computational power when a great level of detail is not needed. In general, different octree grids are employed for the flow and the electrostatic solvers.

Moreover, two-way coupled simulations between the fluid and the particles are possible, meaning that not only the particles would be influenced by the fluid, but also the momentum from the motion of the particles would be transferred back to the fluid.

The software also includes a novel volume of fluid (VoF) module for tracking and locating the free surface [9], and several turbulence models such as k-epsilon, DES and LES to account for the turbulent properties of the flow. It also offers the possibility to create multi-physics simulations such as fluid-structure interactions (FSI) to simulate the interaction of a movable or deformable structure with an internal or surrounding fluid flow [13], or coupling a fluid with electric properties with an existing electromagnetic field.

It is also worth mentioning, that many current industrial applications which involve multi-phase and free surface flows as well as moving and interacting bodies, constitute a challenge for the existing commercial flow solvers on the market, since simulation times are often prohibitive. Having this in mind, IBOFlow was specifically designed to address these limitations by relying on a very efficient implementation while also making use of the huge computational power of modern GPUs. Furthermore, if these features are combined with the innovative Mirroring IB Method, they give IBOFlow superior performance when simulating immersed moving bodies.

The flow solver IBOFlow is part of a larger software system, IPS Virtual Paint [14] also being developed at the FCC. IPS uses IBOFlow libraries in combination with FCC's industrial path planning software, and also includes a user-friendly graphical interface (GUI) for the easy and visual set-up of new spray painting simulations [2] [3].

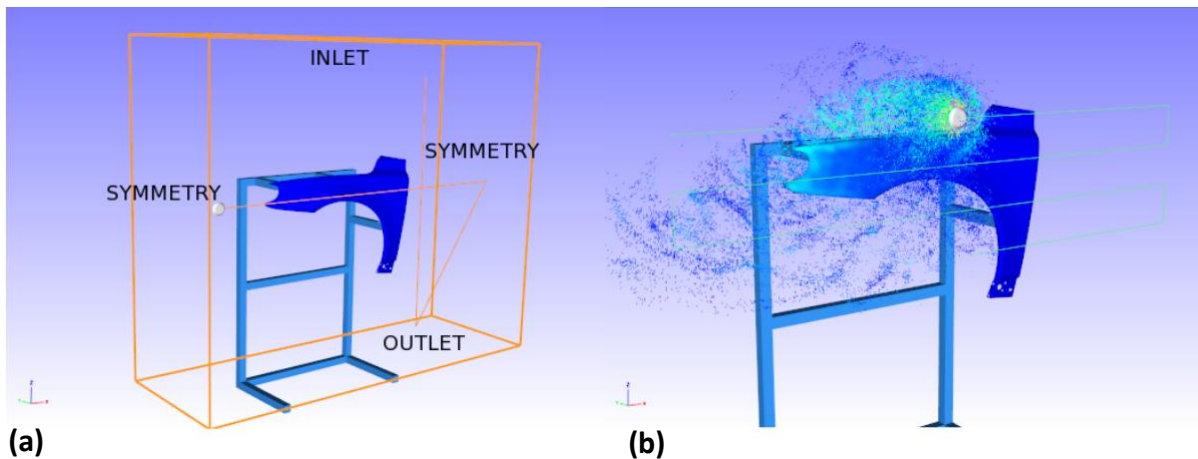


Figure 3.1: The picture to the left (a) shows a computer simulation box with all the boundary conditions set (inlet, symmetry and outlet). The workpiece is a Volvo V60 fender, placed inside the simulation box, and the path specifying the movement of the robot arm holding the applicator bell has been defined. The picture to the right (b) shows an actual snapshot of the simulated painting process. The paint droplets are coloured by the fluid velocity and the fender by the paint deposition thickness.

3.3 Present Approach

Devising integrated simulations of multi-scale and multi-physics phenomena is a very challenging problem in computational physics. After reading section 2.2 explaining the physical phenomena involved in this system, it should be clear how difficult and computationally costly it can be to construct a model which includes all the three regions of an ERBS painting process, and accurately simulates the complex physics present in each region. Several studies have focused in simulating the transport field with already developed airflow and electric fields. These studies usually start the simulations a few centimetres away from the bell, and they use measured particle size distributions and velocity distributions as input conditions for the simulations.

The aim of the present work is to simulate the near-bell region to gain a better understanding of the physics present there. This zone is currently poorly understood, and a great knowledge of the dynamics present there can be gained by creating accurate simulations of that region. This knowledge would allow us to gather information that can later be processed and then used to set-up the initial conditions for coarser simulations. That is to say, it will make it possible to effectively simulate the other regions of the spray painting process, without the necessity to carry out real experiments to find out the input conditions, by performing costly and difficult measurements of the particle sizes and velocities.

The current study can then be divided into two main parts. In the first part, the focus is set on the simulation of the region close to the applicator, no more than a few centimetres away from it. With this purpose, a model was assembled including all the most relevant aspects of the first two regions of an ERBS painting process, that is, the near-bell region and the transport region. These simulations were constructed based solely on input parameters such as the bell rotation speed, quantity of paint

injected, and velocity of the shaping air flow. The values used for these parameters were set to match the measures obtained in the Swerea IVF research laboratories, as explained in section 4.

For the second part of this work, a framework was constructed with the purpose of collecting and analysing particle and fluid data at a plane defined just below the bell. The framework then processes this information and outputs valuable data that can be used as input conditions to run coarser simulations. These simulations can, therefore, cover greater areas and focus on the physics of the transport and target regions of the spray painting, without dealing with the complicated physical aspects of the near-bell region.

4 Experimental Setup

The data for the present work was gathered from experiments performed in the Swerea IVF laboratories, a Swedish research group that encompasses Sweden's industrial research institutes. The experiments were conducted in a research paint booth complemented with a digital controller for ERBS painting. The applicator bell chosen was the new ABB Robobell RB-1000, which uses the internal charging method. The bell has a diameter of 70 mm and a radially serrated edge. Behind the rotary cup, shaping air exits two different sets of annularly arranged pinholes. The inner circular array of pinholes is the secondary shaping air system, and is sometimes called the “purging air”. The outer array of pinholes consists of 36 channels and is the primary shaping air.

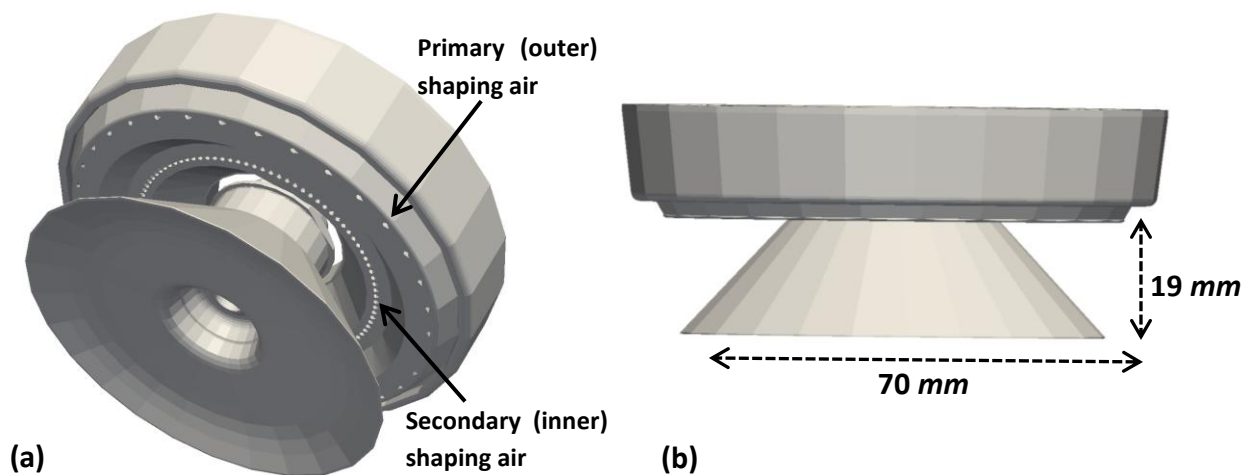


Figure 4.1: Picture (a) illustrates the bell assembly, showing the location of both air shaping systems: the outer (primary) and the inner (secondary). Picture (b) shows the side view of the bell inside the robot arm.

The full report detailing all the configuration scenarios is not included in the present work, but the summary of the technical specifications of the applicator and the actual test conditions can be seen in Table 4.1.

Table 4.1: Main characteristics of the atomiser and test conditions

Bell diameter	70 [mm]
Bell height	21.5 [mm] (19 [mm] to air injectors)
Bell material	<i>Stainless steel. Serrated Edge</i>
Rotary speed	20000 – 40000 [rpm = 1/min]
Liquid flow rate	200 – 650 [ml/min]
Primary shaping air flow rate (outer)	200 – 600 [l/min]
Secondary shaping air flow rate (inner)	200 – 500 [l/min]
High Voltage (internal charging)	0 – 90 [kV]

The optical technique used in this investigation was Laser Sheet Visualization (LSV) by Copper-Vapour Laser (CPL). The short-pulse laser enhances the performance of the high-speed cameras by illuminating the particles with ultra-short pulses of light, eliminating image blur even for droplets moving at very high velocities. An optical arrangement is used to form the output light of the laser into a light-sheet, to take a 2D slice through the turbulent 3D flow, for flow visualization.

For the flow visualization, one high-speed camera was positioned normal to the plane of light sheet taking 1000 images per second. A great number of sequential images were recorded, which allowed the creation of slow motion videos of the behaviour of the spray structure.

For the Particle Image Velocimetry (PIV) measures, which provide instantaneous velocity vector measurements of the flow, two special cameras with very high two-image burst rate were used. That is, they can take two images within an interval of 200 μsec , making it possible to estimate the velocity of the paint droplets by the distance travelled in that time. In order to be able to obtain the three components of the velocity, the cameras were placed with different angles with respect to the normal of the laser light sheet illuminating the flow: one was perpendicular to that plane and the other was at a 45° angle. This measurement process was repeated 100 times for each experiment, resulting in a total of 400 images per setup.



Figure 4.2: Photograph of one of the experiments. The rotating bell is at the end of the robot arm spraying paint onto the target square plate.

The parameters of main interest in this study were the outer and inner shaping air, the liquid flow rate, the bell rotational speed, and the high voltage. Each parameter was varied five times, accounting for a total of 25 different experiments. The following nominal operating conditions, listed in Table 4.2, have been selected to be used as the reference values in this parametric study.

Table 4.2: Simulation parameter values for the atomiser.

Rotary speed	30000 [$rpm = 1/min$]
Liquid flow rate	350 [ml/min] = 5.833×10^{-6} [m^3/sec]
Primary shaping air flow rate (outer)	350 [l/min]
Secondary shaping air flow rate (inner)	350 [l/min]
High voltage	60 [kV]

Below are presented a few sample images obtained with the LSV technique, showing the variations in the paint spray when modifying only one of the parameters. The parameter being modified is set to the maximum test value while the rest of the parameters are kept at the reference value.

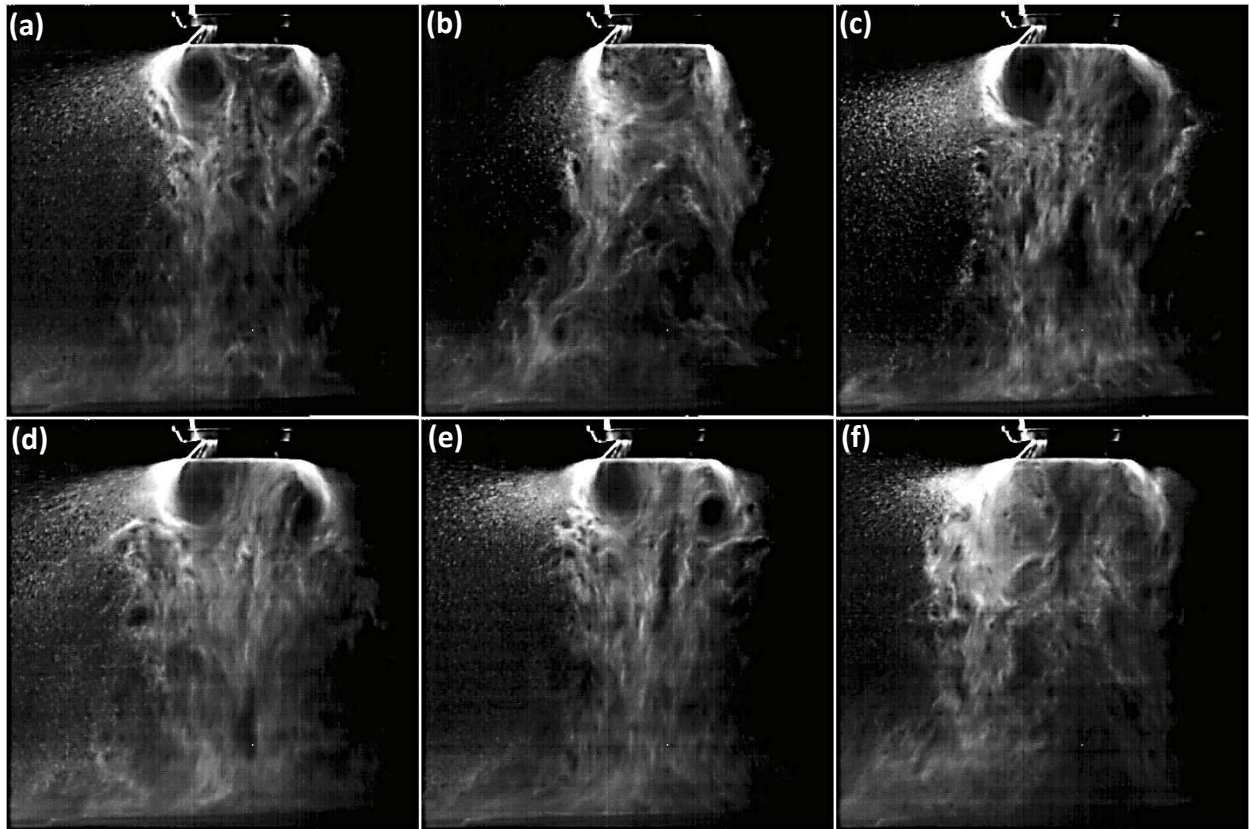


Figure 4.3: Picture showing different test conditions, changing each time only one parameter with respect to the reference case, and setting it to its maximum value: (a) Reference conditions. (b) Outer shaping air rate: 600 l/min. (c) Inner shaping air rate: 500 l/min. (d) Paint flow rate: 650 l/min. (e) Bell rotation speed: 40 rpm. (f) High voltage: 90 kV. Photographs courtesy of Swerea IVF.

Some qualitative observations can be made from these images. Figures (b) and (c) demonstrate the effects of increasing the shaping air systems flow rate. At higher flow rate of the outer (primary) shaping air, the spray cone tends to become narrower. The effect of the inner (secondary) shaping air was less noticeable, except for the extreme combination of using minimum outer shaping air and maximum inner shaping air. The secondary system seems to give more momentum to the paint particles at the edge of the bell and cause bigger air swirls right below the applicator, possibly helping with the atomization process. Figure (d) shows the result of increasing the paint flow rate to 600 l/min. The spray is clearly wider due to the higher spray momentum associated with the increase in the spray mass. This also increases the level of overspray, possibly further aggravated by a larger droplet size. Figure (e) shows the influence of increasing the speed of the bell to 40000 rpm. On the one hand, it is possible to see the effects of the larger centrifugal force, giving a more radial direction to the overspray of bigger particles. However, on the other hand, the main spray cone does not get wider since, the extra centrifugal force also produces a finer atomization, and these smaller particles are easily carried by the air flow. Finally, Figure (f) shows the effect of the high voltage. At the highest voltage, the stronger repelling forces between particles produce a wider and more uniform spray. Additionally, the transfer efficiency close to the target is significantly improved.

5 Computer Simulations Setup

5.1 Part I: Near-Bell Simulations

The computational model of the ERBS painting system was created making direct use of IBOFlow libraries, the CFD solver previously discussed and currently being developed at the FCC. The values of the input parameters were included into different configuration files: “Options” and “Applicators”, to make the set-up of new simulations easier without the inconvenience to recompile the source code every time. The options file contains the parameters concerning the general aspects of the simulation, like the time steps, error tolerances, grid and base cell size, the turbulence and break-up models parameters values, etc. On the other hand, the applicators configuration file comprises the parameters that control the input conditions of the system. That is, it specifies the features of the paint applicator and the shaping air shroud, like the initial positions, total amount of paint used, paint properties, initial paint droplets sizes and velocities distributions, air injector zones and flow speed in each zone, etc.

The computer model for the near-bell simulations was built following the experimental measures summarized in the previous section (see Table 4.1). The following nominal operating conditions, listed in Table 5.1, have been selected to be used as the reference values for input parameters in the computer simulations.

Table 5.1: Simulation parameter values for the atomiser.

Rotary speed	30000 [<i>rpm = 1/min</i>]
Liquid flow rate	350 [<i>ml/min</i>] = 5.833×10^{-6} [<i>m³/sec</i>]
Primary shaping air flow rate (outer)	350 [<i>l/min</i>]
Secondary shaping air flow rate (inner)	<i>Disabled</i>
Voltage	<i>Disabled</i>

The simulation box used has a square base of 160 *cm* side, and is 80 *cm* high. The bell has a diameter of 70 *mm* and an approximate height of 21.5 *mm* from the bottom to its base at the top where it is attached to the robot arm. The bell is placed at 76.5 *cm* from the bottom of the box and the robot arm supplying the paint to the applicator is placed just on top of it. However, the bell’s top goes 2.5 *mm* inside the robot arm, and therefore, the primary shaping air shroud system, placed in the robot, is only 19 *mm* above bell’s bottom edge, as it is depicted in Figure 4.1. The target plate is 45 *cm* wide, 50 *cm* long and 0.2 *cm* thick, and it is placed horizontally and centred in the simulation box exactly 25 *cm* below the bell.

Symmetry boundary conditions were used on the four vertical sides of the simulation box. An inlet boundary condition was used at the upper side of the box with a small uniform downdraft velocity

of -0.38 m/s . Finally, at the bottom side, an outlet boundary condition was used to allow the circulation of the air.

The Cartesian octree grid used internally by IBOFlow was configured with a delta space unit of 2 cm . A total of 4 refinement levels were employed for the area surrounding the bell to get a cell size of $2/2^4 = 0.125 \text{ cm}$ and thus, a high level of detail. Also, 3 refinement levels were used for the area surrounding the target plate. In addition, an extra refinement box also with 3 levels of refinement was defined in the area of interest, namely, the region between the bell and the plate. The octree grid was also configured so that it would automatically refine itself up to 3 levels depending on the value of the gradient of the velocity of the developed flow. In the same manner, the grid coarsens itself if the magnitude of the gradient decreases, and thus, a big level of refinement is no longer needed. In this way, a lot of memory and computational power are saved by using a coarser grid to model the space where changes in the flow direction are small; while still using a very refined grid to model the border of immersed objects, or the areas where turbulent eddies develop. With this refinement options, the initial number of cells in the simulations was 76×10^5 . A picture of the computational mesh showing the automatic refining grid can be seen below in Figure 5.2.

To compute the turbulent three dimensional flow, it was employed the Detached Eddy Simulation (DES) Spalart-Allmaras model, because it is well-suited for complex flow-fields. DES is a hybrid model that combines the best aspects of Reynolds-Averaged Navier-Stokes (RANS) and Large Eddy Simulation (LES) methodologies in a single solution strategy, making the scale-dependence of the model local rather than global. It possess the efficiency of the RANS model in regions close to the walls, and the fidelity of LES away from the wall, thus providing a more accurate description of the three-dimensional, geometry-dependent motion of the fluid.

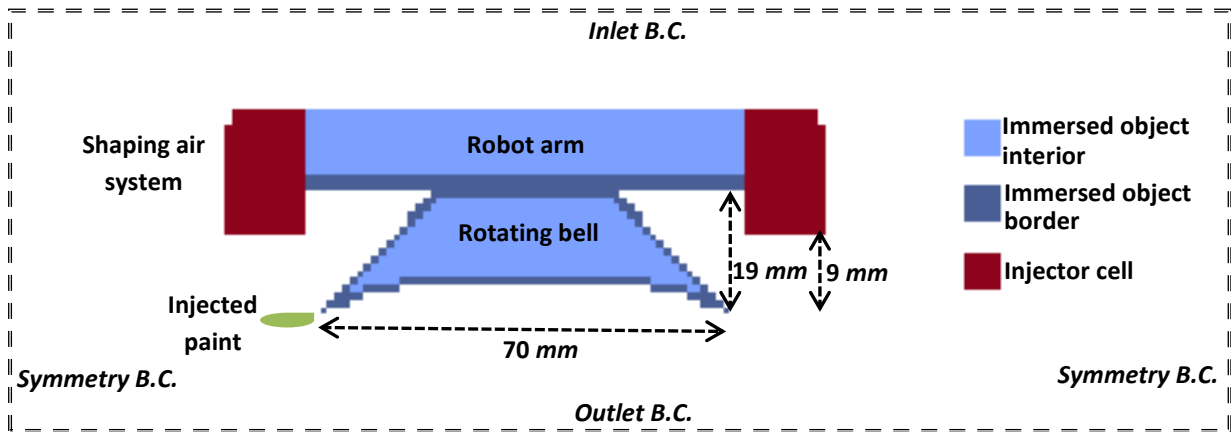


Figure 5.1: A vertical cross section through the volume mesh of the bell area in the computational domain. It is coloured according to the cell type: immersed object interior, immersed object border, or injector cell type.

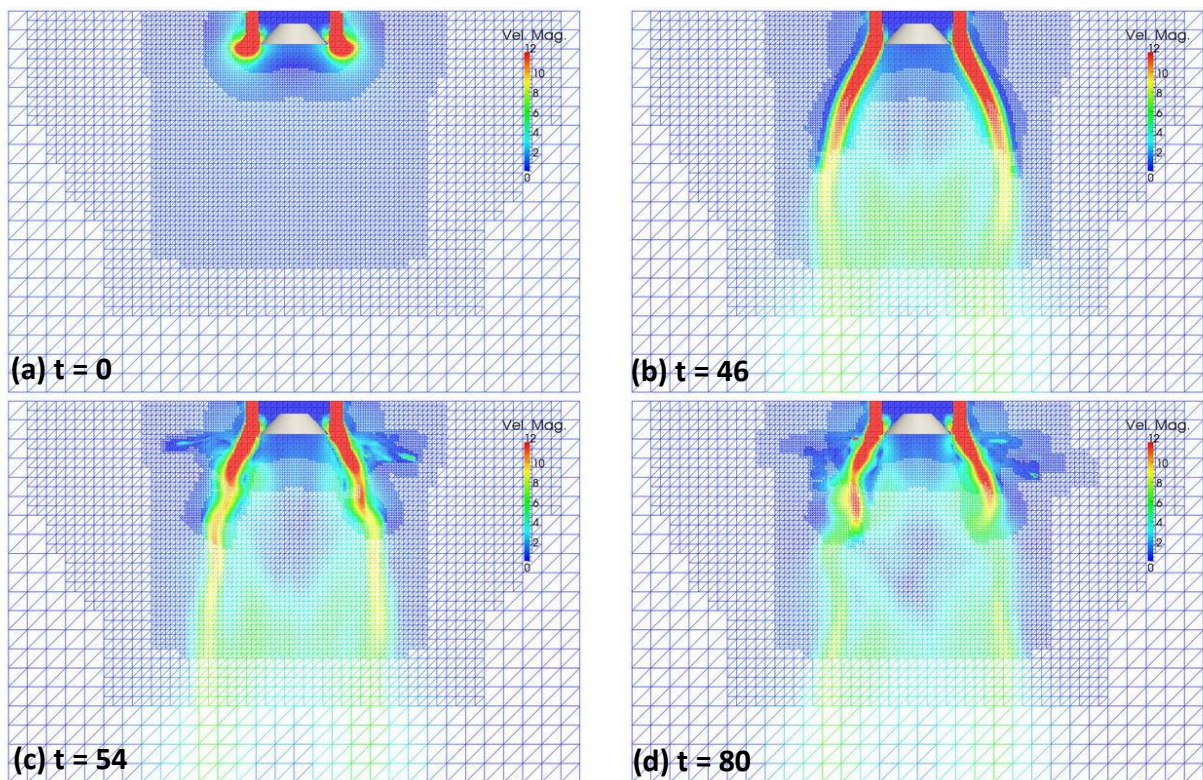


Figure 5.2: Sequence of pictures showing the process of automatic grid refinement at successive time-steps during the simulation. At time-step $t = 50$ the paint applicator begins to spray paint and it is clearly visible the effect it has on the flow: the motion of the paint droplets affect the speed of the main air current, increasing its radial velocity at the edge of the bell and decreasing its magnitude below the applicator. Therefore, more refinements are used radially at the edge of the bell, following the air current created by the particles, and at the same time, the grid coarsens itself further down, where the magnitude of the air velocity has decreased.

The paint particles in the simulation were injected with initial positions uniformly distributed within a cylinder with radii 37 and 38 *mm* from the rotational axis of the bell. That is, between 2 and 3 *mm* away from the actual edge of the bell, at 35 *mm*. The reason for leaving this small gap between the edge of the bell and the paint injection zone was to account for the effects of the primary break-up, which was not modelled explicitly in this type of simulations. Experimental studies of the primary break-up are very difficult, since we cannot prevent or delay the beginning of the secondary break-up phase, and therefore, not much information exists in the literature. As already explained in section 2.2.1, during this first stage of the break-up, the filaments that emanate from the edge of the bell break due to the instabilities caused by their relative velocity with respect to the surrounding air. In the case of near-bell simulation, they already begin with the fragments resultant from the break-up of these initial threads of paint. They are modelled with a lognormal distribution with mean of 100 μm and relative standard deviation of 0.5, which results in a particle size distribution about 10 times in radius (or about 1000 times bigger in volume) than the average final size of the droplets. Moreover, it was estimated that these filaments can lose up to half of their full tangential speed before breaking into smaller fragments [2] [3], and this first stage of the break-up process is completed a few millimetres away from the edge of the bell. This reduction of speed before the secondary break-up occurs was also taken into consideration when setting the initial velocities of the particles. Only 75% of the bell's rim tangential velocity is applied to the particles when they are created. That is a 25% reduction in speed, on average, to account for the velocity lost before the filaments break up.

A particle turbulence model was used to introduce local fluctuations in the velocity field seen by the particles, and allow some turbulent motion. The model creates random fluctuations in the velocity field which are then propagated, correlating them in space and time. Moreover, the magnitude of these fluctuations is then averaged by empirical measures of the turbulence intensity at the different regions. This model performs well and has the advantage of being very fast compared with more advance models.

Finally, the primary shaping air system was included into the simulation. However, recreating the exact conditions for the input of air would have been very difficult, since the air is pumped from the shaping air shroud through 36 different pinholes with 1 *mm* diameter each. For this reason, in the computer simulations, the shaping air was modelled like an inlet ring placed 1 *cm* below the real pinholes, from which the air is injected in a homogeneous way. In order to estimate the dimensions of this ring, the law of momentum conservation was applied, given that the total volume of air injected is an input condition of the simulation, and that the velocity of the air was measured at the place of the inlet ring, 1 *cm* below the pinholes. The momentum conservation law is valid for the motion of any continuum (fluid) as long as the mass of the system is conserved. However, even considering a small compression of the air as a result of the pressure, the momentum conservation law offers a good approximation. The calculations follow:

The rate of volume of air is: $A \cdot |\vec{u}|$ [m^3]

The rate of mass is then: $\rho \cdot A \cdot |\vec{u}|$ [kg]

And the momentum is: $\rho \cdot A \cdot |\vec{u}| \cdot |\vec{u}|$ [$\text{kg} \cdot \text{m}/\text{s}$]

Thus, the sum of the momentums of the air coming out of all the 36 pinholes with individual radius a and air velocity at its exit \vec{u}_1 is:

$$\rho \cdot 36\pi \frac{a^2}{4} \cdot |\vec{u}_1|^2 \text{ [kg.m/s]}$$

And the momentum of the air flowing with speed \vec{u}_2 from a homogeneous ring of radii r_1 and r_2 and is:

$$\rho \cdot \pi(r_2^2 - r_1^2) \cdot |\vec{u}_2|^2 \text{ [kg.m/s]}$$

Since the volume of shaping air injected $S = A \cdot |\vec{u}_1|$ was a parameter of the simulation (i.e. = 350 [l/m] for the reference case), then it was possible to either, estimate the dimensions of the inlet ring to use (r_1 and r_2) based on empirical measures of the air velocity at that place (\vec{u}_2); or, the other way around. That is, fixing the radii values of the ring in order to estimate the air velocity.

The last step consisted in directing the air flowing from the shaping air ring in the correct direction. According to the measures, the direction was approximately 30° downwards and backwards in the plane tangential to the bell's edge. That is, considering the plane tangential to the edge of the bell, the air pinholes were directed 30° from the negative Z axis, in the direction opposite to the rotation of the bell. They were also pointing slightly inwards towards the rotational axis of the bell, that is, about 1° from the negative Z axis, in the negative radial direction. Thus, considering:

$$\theta = 30^\circ \text{ (Vertical towards tangential direction)}$$

$$\varphi = 1^\circ \text{ (Vertical towards radial direction)}$$

The final projection of the velocity was:

$$u_z = -|\vec{u}_2| \cos \varphi \sin \theta \text{ [m/s]}$$

$$u_{tangential} = |\vec{u}_2| \cos \varphi \cos \theta \text{ [m/s]}$$

$$u_{radial} = -|\vec{u}_2| \sin \varphi \text{ [m/s]}$$

5.2 Part II: Analysis Framework

For the second part of the project, a framework was constructed using Python, to analyse the output files of the near-bell simulations in order to collect and process particle and fluid statistics. This software tracks the individual particles, collecting their properties like positions, velocities, masses and radii, as they move along the flow. A special interest, however, resides in the instant when the particles cross through a predefined horizontal plane 2.5 cm below the bell. This plane is divided into concentric circular regions, with common centre in the point of intersection with the rotation axis of the bell. The information gathered from the particles while crossing the plane is then averaged over the defined circular regions to get distributions concerning the paint flow, droplet size, and velocity of the particles as a function of their radial distance to the rotation axis.

Fluid statistics are processed too, in a similar manner, on a plane placed 1.5 *cm* below the bell, that is, 1 *cm* above the plane where the particles are processed. The fluid velocity of the air over this plane is also averaged over circular regions to obtain the distribution for the air velocity, also as a function of the distance to the bell's axis of rotation.

All this data is then structured by the Python script into the output format of the Applicator configuration file, as described in the previous section, and saved to disk, so that it can later be used as input for other IBOFlow simulations. In other words, what the python script does, is to sample the particle statistics and the fluid statistics over two different horizontal planes below the bell, and uses that information to build a configuration file in which those planes are specified as inlets. That means that the fluid statistics collected define the new "air injector" properties, while the particle statistics constitute the new "paint injector" characteristics. This allows the set-up and run of a very different type of simulations by using these parameters as input conditions, as it will be explained in the following section, 5.3.

In addition to creating the input conditions for other IBOFlow simulations, the Python code also creates several plots that help visualize and further understand the dynamics of the particles and the fluid close to the applicator. In several cases this data can also be saved to disk in the very convenient VTK format for visualization in Paraview [15]. These plots are presented in the Results section.

5.3 Part III: Far-Field Simulations

The source code for these simulations is in fact very similar to the code used by the near-bell simulations. However, in this case, the idea is to create a coarser mesh with larger grid cells on average, and to avoid simulating the complex physics present in the near-field, close to the bell. Nonetheless, for testing and validation purposes, it was still better if the same parameters values were used in both types of simulations in order to be able to compare the results afterwards.

With this purpose, the computational domain was built having the same dimensions as before, and the objects were placed at the exact same positions. However, in the far-field simulations the applicator area does not have an important role anymore, except for the formation of the electric field between the bell and the target. Alternatively, the air and the paint injectors are simply circular regions, defined over specific planes, as indicated in the applicator configuration file obtained from the Python analysis framework. As it was explained previously, the input parameters such as the particle velocity, mass and radius, and the air velocity, were taken from the sampling performed by the Python script on the near-bell simulations.

The boundary conditions used for these simulations were the same as for the near-bell case, that is, symmetry boundary conditions were set on the four sides of the simulation box, an inlet boundary condition was set at the upper side with the same air current as before of -0.38 *m/sec*, and an outlet boundary condition was set at the bottom of the box. Notice that in this case, the planes where the air and the paint were injected can also be considered as inlet boundary condition planes. The only difference is that they have non homogeneous injection rates and properties, since these features

depend on the distance from the specific injection zone to the rotational axis of the bell at the middle of the XY plane of the simulation box.

The Cartesian octree grid used to model the computational domain was also configured with the same base delta space unit of 2 *cm*, and the number of refinements used was also kept at 3 for the refinement box in the zone between the injector planes and the target plate.

6 Results and Discussion

6.1 Near-Bell Simulations

To validate the computer near-bell simulations the first step was to look at the development of the flow and compare it with the real experiments performed in the lab. The first parameter studied was the inner shaping air flow rate. Figure 6.1 below compares vertical cross section images of the PIV measures (in the first row) with instantaneous snapshots of the fluid velocity in the computer simulations with and without particles (in the second and third rows respectively), and also with instantaneous images from the high speed cameras (in the fourth row).

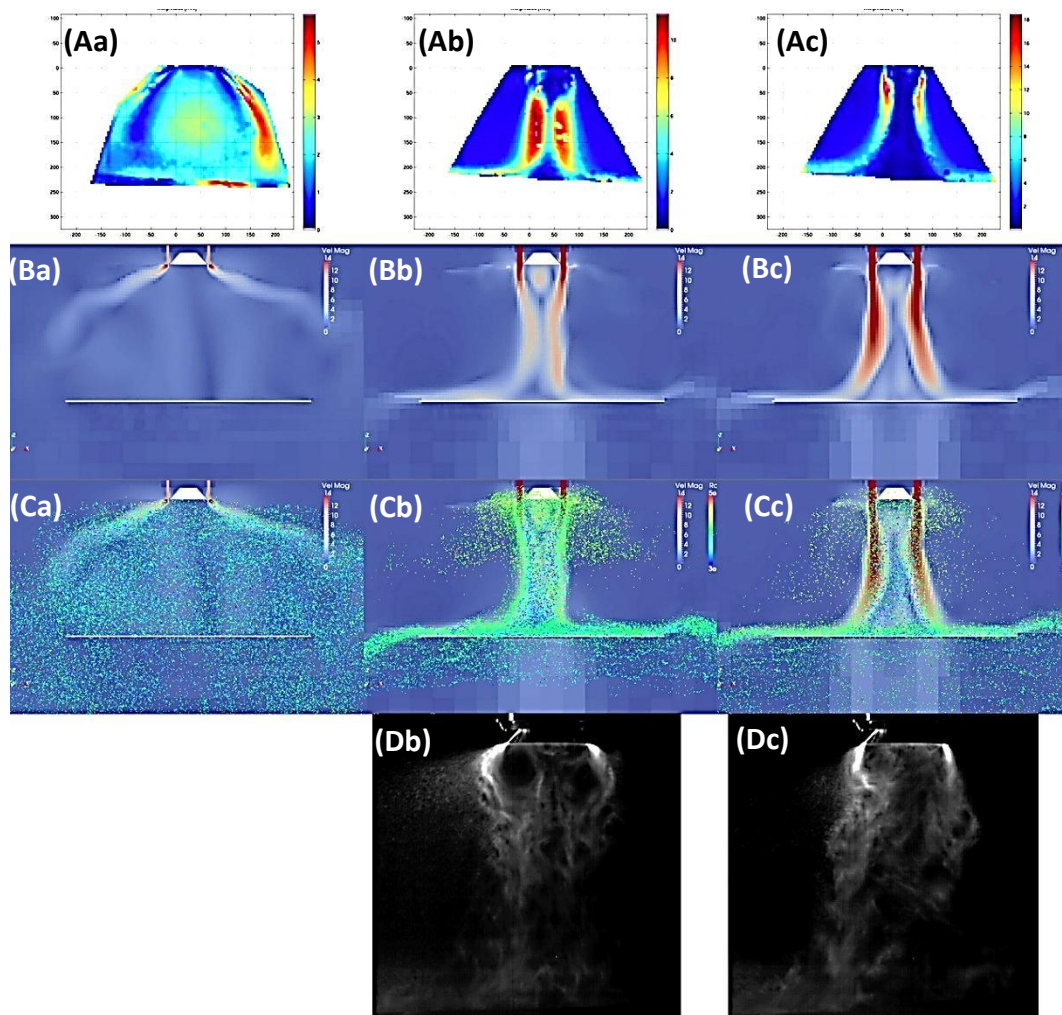


Figure 6.1: Shaping air flow rate parameter study. The three columns correspond respectively, from left to right, to: (a) 200 l/min, (b) 350 l/min, and (c) 600 l/min. The four rows correspond respectively, from top to bottom, to: (A) PIV measures, (B) the simulation's airflow velocity magnitude, (C) the simulation's airflow velocity magnitude with particles, and finally, (D) the images from the high-speed camera.

It can be observed from these images how much the flow development in the computer simulations resemble the PIV measurements for different shaping air flow rates. For the first case of 200 l/min the momentum of the particles is too big compared with the momentum of the flow of air, and therefore the spray cone expands to a great extent. In the second case, for 350 l/min , the airflow cone gets narrower, even more than the diameter of the bell itself, shrinking towards the rotating axis of the applicator. This phenomenon is only observable for the “right” amount of air, since when the shaping air is increased to 600 l/min , the airflow cone expands again. In this case the expansion is caused by the big reflux of air in the centre, caused by the air hitting the target plate.

The second parameter studied concerned the paint flow rate. Figure 6.2 below shows the comparison of different cross section images for different rates of injected paint. The first row of images are the PIV measures, the second rows shows instantaneous snapshots of the air velocity and the particles in the computer simulations, and in the third row are the high-speed camera pictures.

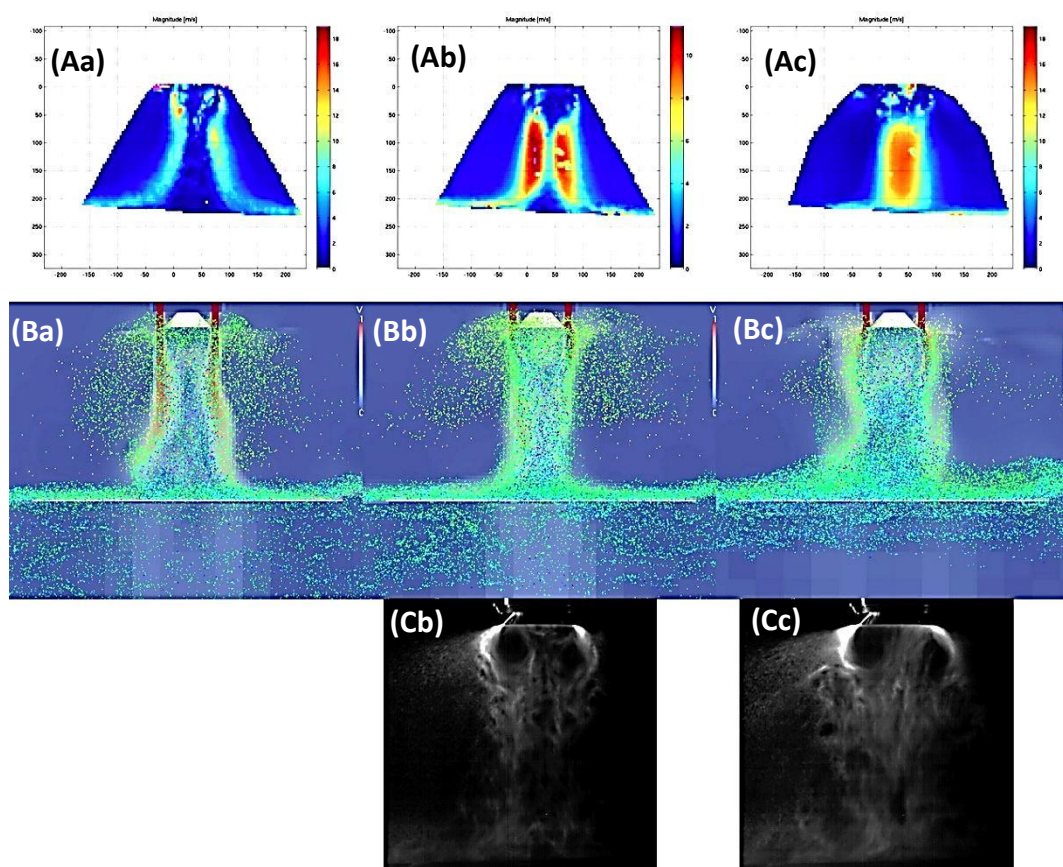


Figure 6.2: Paint flow rate parameter study. The three columns correspond respectively, from left to right, to: (a) 200 ml/min, (b) 350 ml/min, and (c) 650 ml/min. The four rows correspond respectively, from top to bottom, to: (A) PIV measures, (B) the simulation’s airflow velocity magnitude with particles, and (C) the images from the high-speed camera.

Again, the computer simulations show a good resemblance to the PIV measurements. For the case of 200 ml/min the air cone tends to expand, while for the case of 350 ml/min , the base case, the airflow shrinks towards the middle, as was already seen in the previous figure. In the last case, for

650 ml/min of paint, it is easier to compare the computer simulation with the high-speed image. It is possible to see that the cloud of particle droplets is actually wider, but at the same time, there are a large number of particles in the middle of the spray cone. This high density of particles in the centre is what caused the laser PIV measures to show a dense column in the middle of the plot.

The third and last parameter study was the rotational speed of the applicator bell. Figure 6.3 shows the usual comparison between the PIV measures (first row), the computer simulations (second row) and the high-speed camera pictures (third row).

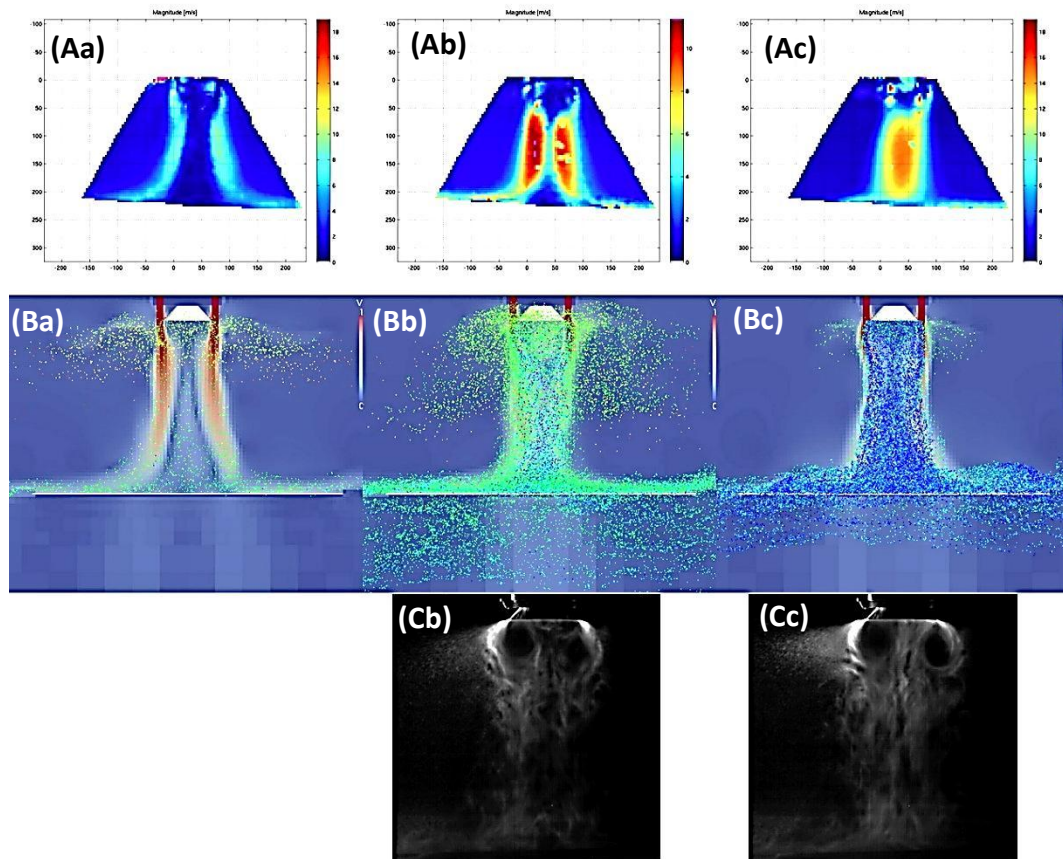


Figure 6.3: Applicator rotation speed parameter study. The three columns correspond respectively, from left to right, to: (a) 20 krpm, (b) 30 krpm, and (c) 40 krpm. The four rows correspond respectively, from top to bottom, to: (A) PIV measures, (B) the simulation's airflow velocity magnitude with particles, and (C) the images from the high-speed camera.

As with the previous parameters, the similarity between the PIV measurements and the computer simulations is evident. In the first case, where the bell is rotating only at 20 krpm, the atomization is poor and the mean paint droplet size is much bigger. That is the cause for the large overspray close to the edge of the bell seen in the computer simulation picture. On the other hand, in the case of 40 krpm the very high speed of the bell creates very small droplets which are easily carried by the airflow, producing the dense column of paint particles seen in the computer simulation image. Exactly as in the case of 650 ml/min paint flow rate, this high density of paint droplets in the centre is the reason for the plot of PIV measures appearing like a single column in the middle.

6.2 Analysis Framework

In this section the results from the analysis framework for the reference case are presented. The analysis was run considering 100 simulation time-steps, and the output plots generated are shown next.

Figures 6.4 and 6.5 below illustrate the processing performed on the air velocities at the sampling plane, 1.5 cm below the bell. Figure 6.4 shows a quiver plot of the air velocities at the sampling plane before being processed. Figure 6.5 shows the resulting air velocity after calculating the radial averages and filtering the final containers with less than 10% of the total amount of air. These values for the velocity of the air are the ones employed when building the applicator file for the far-field simulations.

Figure 6.6 and Figure 6.7 show the trajectories of the particles coloured by the particle radius and by the particle velocity, respectively. From these images it is easy to see how the big particles manage to cross the strong downwards flow coming from the shaping air system at the edge of the bell, and therefore, unaffected by the downdraft, they describe a trajectory where they move straight in the radial direction until their velocities decrease considerably and then they just simply fall down. The small particles on the other hand, are easily carried by the downwards flow, and they are usually located at the centre of the spray cone. From the velocity plot with logarithmic scale it can also be observed how quickly the velocities of the particles decrease. They only have very strong speeds right at the edge of the bell. Then, their mean velocity is very close to the velocity of the downdraft air for the particles being carried by the airflow.

Figure 6.8 below shows the particles while they cross the paint sampling plane, 2.5 cm below the bell. In the image, the size and colour of the particles is based on their radii, on a logarithmic scale, and the size and direction of the arrows represent their velocity vectors. It is possible to observe here again how the small particles are located in the middle and have larger velocity vectors. Big particles may also have large velocity vectors, but only in the radial direction, and only if they are sampled really close to the bell. The radial containers along which the particles are averaged are also visible in the image.

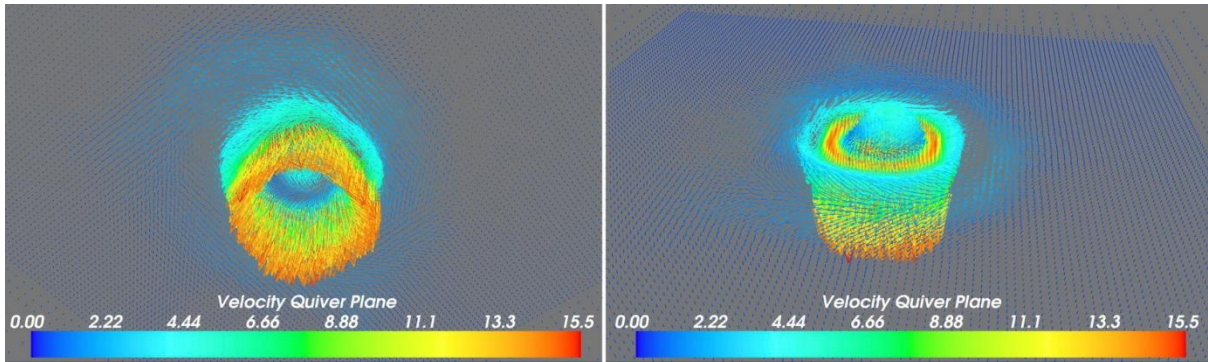


Figure 6.4: Quiver plot showing the air velocity vectors in the air sampling plane, 1.5 cm below the bell.

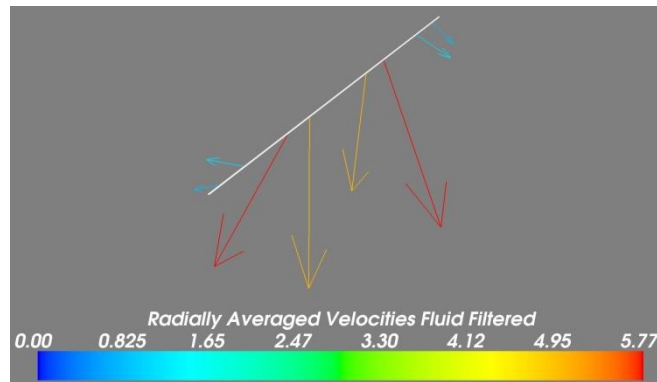


Figure 6.5: Quiver plot showing the radially averaged and filtered air velocities of the air in the sampling plane. These values are the ones used to construct the air inlet plane injecting air in the far-field simulations.

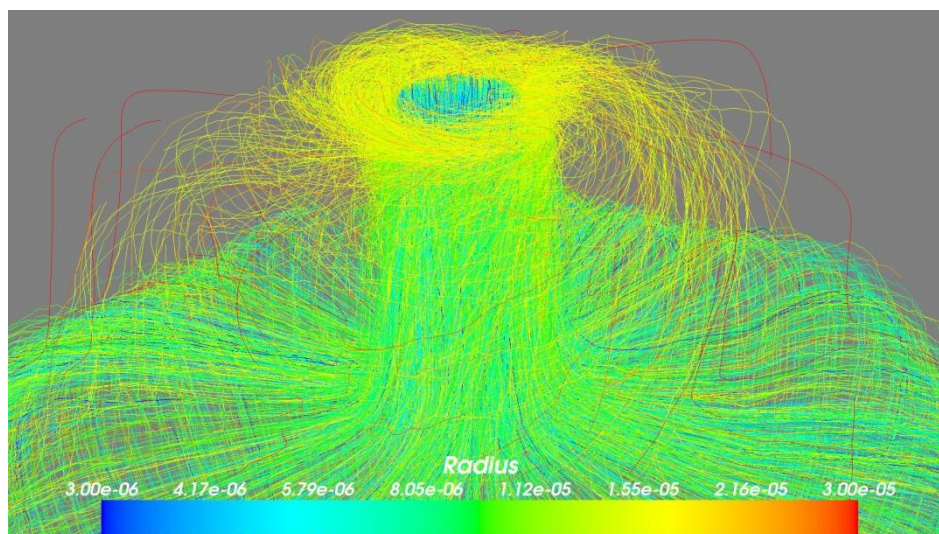


Figure 6.6: Particles trajectories coloured by their radius.

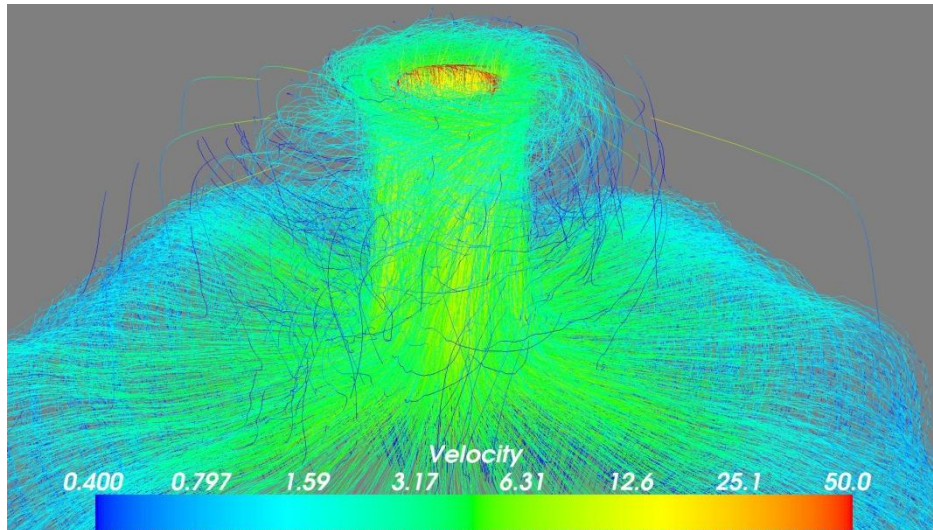


Figure 6.7: Particles trajectories coloured by their velocities.

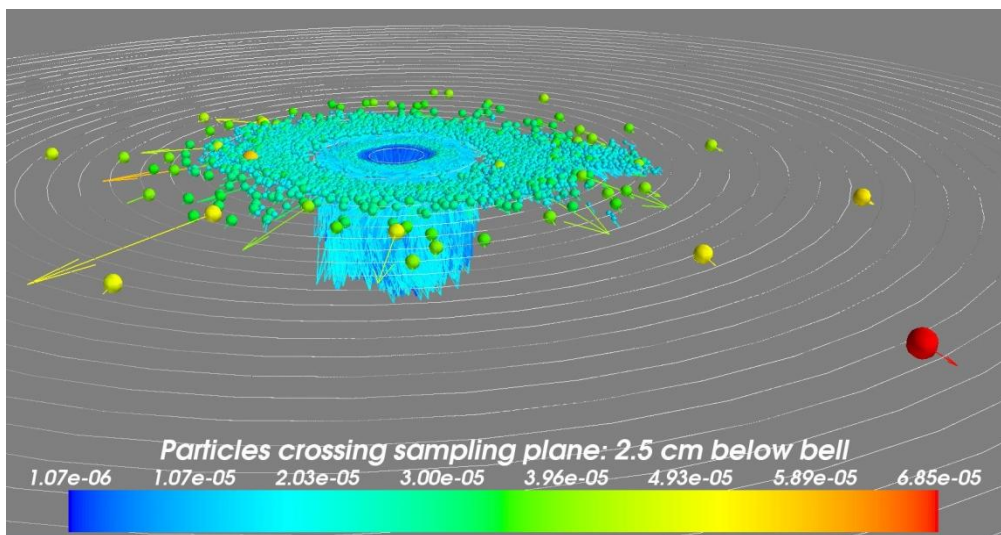


Figure 6.8: Particles crossing the sampling plane 2.5 cm below the bell. The particles size and colour depends on their radii, and the size and direction of the arrows represent their velocity vectors.

Figure 6.9 shows the particle statistics sampled over the plane 2.5 cm below the bell. All the plots are averaged radially, and so the X axis represents the distance to the rotational axis of the bell. The first plot shows the magnitude of each velocity component. It can be seen the huge angular velocity at the edge of the bell, and how quickly it decreases. The second plot shows the average diameter of the particles impacting the plane and it can be seen that the bigger particles impact on the plane further away from the bell's edge. The third plot is the mass flow, and the fourth plot shows the number of particle hits.

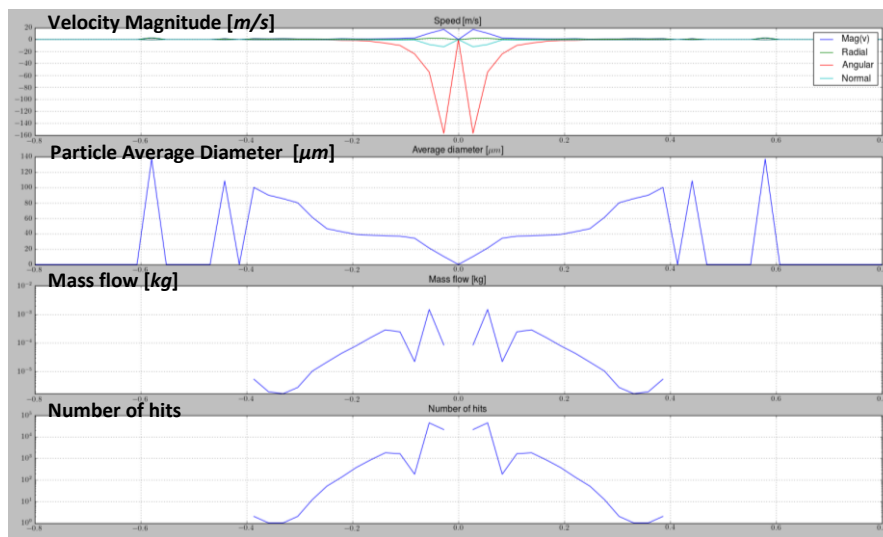


Figure 6.9: Particle statistics sampled over the plane. From top to bottom the plots show the plots show: (1) the magnitude of each velocity component, (2) the average particle diameter, (3) the mass flow, and (4) the number of hits.

Finally, this analysis framework also track the particles over the three dimensional space. A grid is defined over which the particle statistics are calculated and averaged. In order to account for possible jumps of a particle over certain grid cells from one time-step to the next, a ray tracing algorithm was implemented. These figures can be seen below. Figure 6.10 (left) shows the average velocities of the particles, Figure 6.11 shows the average number of particles, and Figure 6.12 shows the average turbulence intensity. Figure 6.10 also compares the average velocity with the PIV measures (right) to appreciate the similarity both in shape and magnitude.

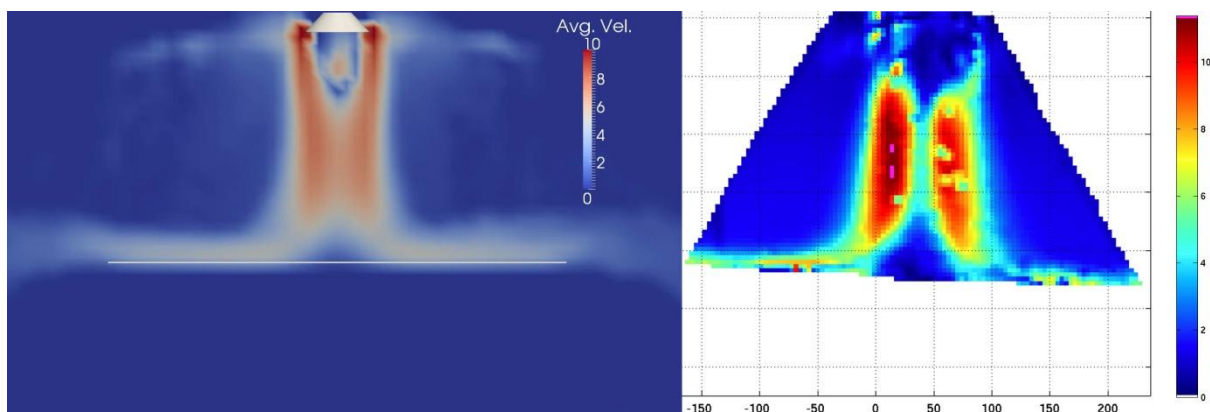


Figure 6.10: Average particle velocity (left) and PIV measurements (right).

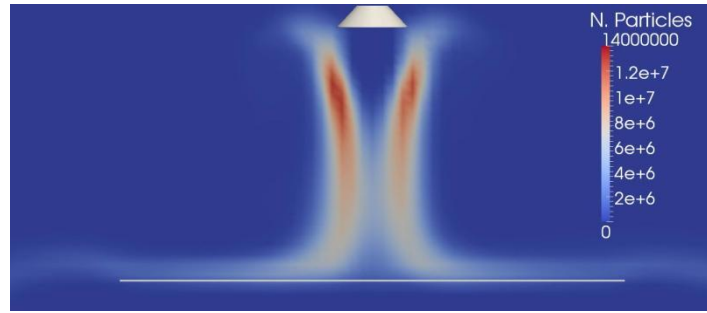


Figure 6.11: Average number of particles.

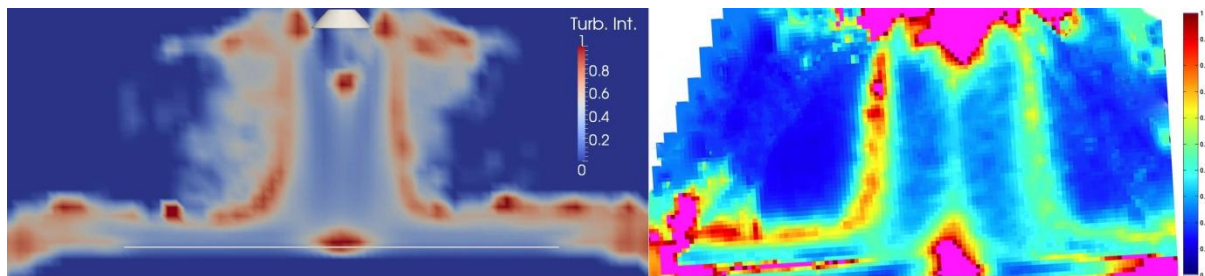


Figure 6.12: Average turbulence intensity (left) and PIV measurements (right).

6.3 Far-Field Simulations

The far field simulation was constructed as specified in section 5.3 however the validity of the results have yet to be tested. Figure 6.13 below shows an early snapshot of the development of the flow using the inlet injector planes generated with the Python framework analysis, to inject both the air and paint into the simulation. Since this is a work in progress, it will be discussed further in the future work section.

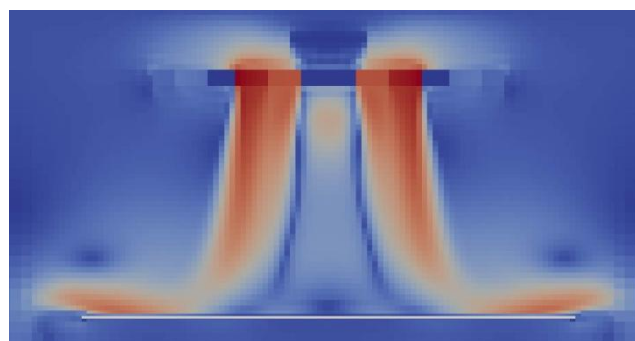


Figure 6.13: Snapshot of the air flow in the far-field simulation. The injectors air and paint injectors were generated by the Python analysis framework.

7 Conclusion

In the present work, a rotary-bell spray painting system was successfully modelled and simulated. Simultaneously, a parametric study of an electrostatic rotary-bell spray painting system was carried out at the Swerea IFV laboratories using the laser light sheet visualization technique. From these methodical trials important features of the system were identified, and a better understanding of the paint spray structure and the transfer process was gained. The results showed that the rotational speed of the bell has a strong effect on the atomization of the paint, and that the shaping air flow rate, the paint flow rate, and the high voltage, significantly affect the spray transport.

Subsequently, and based on these measures, a parametric study on the computer simulations was performed, setting the values of the parameters to match those of the experimental setups. For each configuration, the development, shape, structure, and behaviour of both, the air flow and the spray cone in the computer simulations were compared to that of the real trials to look for validation. This comparison was performed for three of the main parameters of the system, namely, the shaping air flow rate, the paint flow rate, and the rotational speed of the bell; and all of them were found to be in very good agreement with the laboratory experiments.

The framework created to analyse the output data of the simulations also provides detailed information and statistics concerning the particles and the fluid. This information helps to better understand the transport process, which contributes to improve the numerical simulations. Additionally, it can also be used in future model development and validation. Moreover, based on these statistics, the framework creates the configuration files used as input for the coarser and larger simulations.

The automatically generated applicator files were successfully used to run far-field simulations. However, these results are yet to be validated, and therefore they are discussed in the Future Work section.

8 Future Work

Since this is an on-going work much work has yet to be done. Furthermore, many improvements would also be desirable in order to improve the level of accuracy of the simulations and their performance.

First of all, parameter studies still need to be carried out concerning the far-field simulations. The first step would be to validate them comparing their flow development and behaviour with the corresponding near-bell simulation from which the applicator files were created.

The computational model also requires two important additions to be in accordance with the experimental setups. The first one is very simple and is the inclusion of the inner shaping air system, although as shown by the experiments, a big change in the flow development is not to be expected. The second one is also not complex in terms of implementation but it will require a considerable amount of computational power. This is the inclusion of the electric repellent forces between particles, given that the experiments showed the significant effect of the high voltage, especially close to the bell.

Moreover, it could also be included a model to simulate the primary breakup process at the bell's edge. This feature should not have a direct impact in the results of the numerical simulations if the initial parameters used for the secondary breakup are correct, but it would complete the modelling of the spray painting process.

Concerning the improvements which could be made regarding the internal implementation and the data structures of the simulations, there is one addition that is believed could be particularly important in improving the results. That is the employment of a cylindrical mesh along with cylindrical coordinates. Curvilinear coordinates produce an inherent grid refinement: the closer the cells are to the object the smaller the grid cells become. Therefore, the use of curvilinear grid cells would allow getting a high level of detail close to the edge of the bell while at the same time requiring a substantially lower number of cells. Moreover, this type of cells forming a cylindrical structure can be defined with a very small size in the radial dimension, where a high level of detail is needed, and they can be large in the angular dimension, where more coarse approximations can be afforded due to the cylindrical symmetry.

Last but not least, many more empirical experiments need to be carried out. Advanced measurement devices and techniques should be used so as to get good quality measures which can be trusted to build the computer simulations based on them, and to validate the results. In particular, measures of the electric field and the particles charges are required. Additionally, improved measures for the airflow speed in the regions very close to the bell, and right below the air injectors are highly important. Moreover, horizontal cross-section images should be performed by placing the laser sheet between the bell and the target, since in the current study only vertical cross-section images were taken. Finally, paint thickness profiles experiments need also to be run to be able take them as another point of reference for the validation of the simulations.

Bibliography

- [1] D. Kim and P. Moin, "Numerical simulation of the breakup of a round liquid jet by a coaxial flow of gas with a subgrid Lagrangian breakup model," 2011.
- [2] R. Rundqvist, A. Mark, B. Andersson, A. Ålund, F. Edelvik, S. Tafuri and J. S. Carlson, "Simulation of Spray Painting in Automotive Industry," Springer Berlin Heidelberg, 2010, pp. 771-779.
- [3] A. Mark, B. Andersson, S. Tafuri, K. Engström, H. Söröd, F. Edelvik and J. S. Carlson, "Simulation of Electrostatic Rotary Bell Spray Painting in Automotive Paint Shops," in *ICLASS 2012, 12th Triennial International Conference on Liquid Atomization and Spray Systems*, Heidelberg, Germany, September 2-6, 2012.
- [4] B. Andersson, S. Jakobsson, A. Mark, F. Edelvik, J. S. Carlson, V. Golovitchev and L. Davidson, "Modified TAB Model for Viscous Fluids applied to Breakup in Rotary Bell Spray Painting," in *ICLASS 2012, 12th Triennial International Conference on Liquid Atomization and Spray Systems*, Heidelberg, Germany, September 2-6, 2012.
- [5] M. R. Maxey and J. J. Riley, "Equation of motion for a small rigid sphere in a nonuniform flow," *Physics of Fluids*, vol. 26, no. 4, pp. 883-889, 1983.
- [6] L. Schiller and A. Neumann, "Über die Grundlegenden Berechnungen bei der Schwerkraftaufbereitung," *Ver. Deutsch. Ing.*, vol. 77, pp. 318--320, 1933.
- [7] R. Clift, J. R. Grace and M. E. Weber, *Bubbles, Drops and Particles*, New York: Academic Press, 1978.
- [8] S. Laín and C. A. Grillo, "Comparison of turbulent particle dispersion models in turbulent shear flows," *Brazilian Journal of Chemical Engineering*, vol. 24, pp. 351 - 363, 09 2007.
- [9] A. Mark, R. Bohlin, D. Segerdahl, F. Edelvik and J. Carlsson, "Process Simulation and Automatic Path Planning of Sealing Application in Automotive Paint Shops," in *Swedish Production Symposium*, 2012.
- [10] "IBOFlow," [Online]. Available: <http://www.industrialpathsolutions.com/future-modules/ips-iboflow>.
- [11] A. Mark, R. Rundqvist and F. Edelvik, "Comparison Between Different Immersed Boundary Conditions for Simulation of Complex Fluid Flows," *Fluid Dynamics & Materials Processing*, vol. 7, no. 3, pp. 241--258, 2011.
- [12] A. Mark and B. v. Wachem, "Derivation and Validation of a Novel Implicit Second-Order Accurate Immersed Boundary Method," *Journal of Computational Physics*, vol. 227, no. 13, pp. 6660-6680, June, 2008.

- [13] E. Svenning, A. Mark and F. Edelvik, "Simulation of fluid structure interaction with free surface flows," in *The 17th European Conference on Mathematics for Industry*, Lund, Sweden, July 17-23, 2012.
- [14] "IPS Virtual Paint," [Online]. Available: <http://www.industrialpathsolutions.com/future-modules/ips-virtual-paint>.
- [15] "ParaView - Open Source Scientific Visualization," [Online]. Available: <http://www.paraview.org/>.
- [16] J. Domnick, A. Scheibe and Q. Ye, "The Electrostatic Spray Painting Process with High-Speed Rotary Bell Atomizers: Influences of operating conditions and target geometries," in *Proceedings of 9th International Conference on Liquid Atomization*, 2003.
- [17] Q. Ye, J. Domnick and A. Scheibe, "Numerical simulation of spray painting in the automotive industry," in *Proceedings of 1st European Automotive CFD Conference*, 2003.
- [18] Q. Ye, J. Domnick, A. Scheibe and K. Pulli, "Numerical Simulation of Electrostatic Spray-painting Processes in the Automotive Industry," Springer Berlin Heidelberg, 2005, pp. 261-275.
- [19] M. A. Patterson and R. D. Reitz, "Modelling the effects of fuel spray characteristics on Diesel engine combustion and emission," *SAE paper 980131*, 1998.
- [20] C. Narayanan, D. Lakehal, L. Botto and A. Soldati, "Mechanisms of particle deposition in a fully developed turbulent open channel flow," *Physics of Fluids*, vol. 15, no. 3, pp. 763-775, 2003.
- [21] K.-S. Im, M.-C. Lai, Y. Liu, N. Sankagiri, T. Loch and H. Nivi, "Visualization and Measurement of Automotive Electrostatic Rotary-Bell Paint Spray Transfer Processes," *Journal of Fluids Engineering*, vol. 123, no. 2, pp. 237-245, 2001.
- [22] K.-S. Im, M.-C. Lai, S.-T. J. Yu and J. Robert R. Matheson, "Simulation of Spray Transfer Processes in Electrostatic Rotary Bell Sprayer," *Journal of Fluids Engineering*, vol. 126, no. 3, pp. 449-456, 2004.
- [23] J. Domnick, A. Scheibe and Q. Ye, "The Electrostatic Spray Painting Process with High-Speed Rotary Bell Atomizers: Influences of operating conditions and target geometries," in *Proceedings of 9th International Conference on Liquid Atomization*, 2003.
- [24] J. Amanatides and A. Woo, "A Fast Voxel Traversal Algorithm for Ray Tracing," in *In Eurographics 1987*, 1987.
- [25] B. Andersson, S. Jakobsson, A. Mark, F. Edelvik and L. Davidson, "Modeling Surface Tension in SPH by Interface Reconstruction using Radial Basis Functions," in *Proceedings of the 5th International SPHERIC Workshop*, Manchester (U.K.), 2010.